Nano Energy 94 (2022) 106908

Contents lists available at ScienceDirect

Nano Energy

journal homepage: www.elsevier.com/locate/nanoen

A facile method to enhance the flexibility and triboelectric output of PDMS using ionic liquid-coated single-wall carbon nanotubes

Xiaoyue Zhao, Zoubeida Ounaies *

Department of Mechanical Engineering, The Pennsylvania State University, University Park, PA 16802, United States

ARTICLE INFO

Keywords:
Energy conversion
Triboelectric output
Polymer composite
Ionic liquid
Carbon nanotube

ABSTRACT

Energy harvesting devices based on triboelectric effect have gained much attention recently due to their significant potential in low-frequency applications, especially in wearable electronics. To enable these devices, flexible materials with relatively high electrical conductivity and large triboelectric output are needed. In this study, a PDMS composite is fabricated using embedded ionic liquid (IL) coated single-wall carbon nanotubes (SWCNTs). The ratio of IL to SWCNTs is tuned to achieve the desired material properties for wearable triboelectric nanogenerators. The SWCNT-IL-PDMS (IL: SWCNT= 20:1) composite exhibits a relatively high electrical conductivity (0.004 S/m) and an enhanced triboelectric output compared to unmodified PDMS. Specifically, the open-circuit voltage (V_{oc}) and the short-circuit current (I_{sc}) are increased by three folds. The relatively high electrical conductivity enables the composite to transfer charges without electrodes and reduces the internal impedance of triboelectric nanogenerators. The flexibility of the composite is also improved, as demonstrated by the decrease in both the tensile and compressive elastic moduli. In addition, the mechanism behind the change in electrical properties and triboelectric output is proposed and discussed in this paper. Specifically, the increase in the dielectric constant and electrical conductivity of the composites with IL is likely due to the better dispersion of SWCNT in the polymer matrix, and the change in the triboelectric output is a result of (1) the trade-off between dielectric constant and electrical conductivity, and (2) the shifting of triboelectric polarity with the addition of IL. This study not only provides a facile method to simultaneously increase the flexibility, electrical conductivity, and triboelectric output of polydimethylsiloxane (PDMS), but also generalizes the approach and paves the way to explore new flexible and electrically conductive materials for wearable triboelectric nanogenerators.

1. Introduction

Energy harvesting materials and systems capable of powering small-scale electronic mobile devices autonomously have emerged as a prominent research area with many rapid developments, in particular in the context of Internet of Things (IoT) [1–5]. This interest arises from the fact that conventional power supply technologies have difficulties in powering widely distributed and mobile devices, which are major components in IoT. For example, the grid needs hard wires to connect with electronic devices which limits the mobility of the device; similarly, batteries have limited lifetime, which makes monitoring and replacing them challenging, particularly when they are widely distributed and in hard-to-access locations. In addition, disposing of depleted batteries is a challenge due to their chemical components and the potential for environmental pollution [1,6]. Among the different energy harvesting systems developed recently, triboelectric nanogenerators have gained particular attention since they are flexible, portable, cost effective and light weight [5,7–12]. Moreover, triboelectric nanogenerators are well-suited for harvesting ambient low-frequency energy (< 5 Hz) that is otherwise wasted in our daily lives [13,14]. These characteristics make triboelectric nanogenerators not only applicable in harvesting mechanical energy from human activities, such as human walking [15–18], respiration [19–21], motor vibration [22–24], tire rotation [25–27], but also suitable for harvesting energy from nature, such as wind [28–31], rain drop [32–34] and ocean [14,35,36]. To date, the power density and efficiency of triboelectric nanogenerators have reached up to 500 W/m^2 [37] and 85% [38] respectively, which can meet the power demand of many small wearable electronics, such as digital watches [39–41], human health monitors [21,42,43], pedometers [44–46] and remote keyless entry modules [43,47].

* Corresponding author.
E-mail address: zxo100@psu.edu (Z. Ounaies).

https://doi.org/10.1016/j.nanoen.2021.106908
Received 20 October 2021; Received in revised form 28 December 2021; Accepted 29 December 2021
Available online 31 December 2021

There are challenges that currently stand in the way of the wide use of triboelectric nanogenerators. For example, the inherent mechanism of triboelectricity is still poorly understood, and is described mainly through qualitative or empirical relationships; also, the intrinsic capacitive behavior of triboelectric nanogenerators results in a high impedance and a low current output, which hinders their direct use as power supplies. Typically, the impedance of triboelectric nanogenerators ranges from tens of mega-ohm to giga-ohm [8,44,48], while the impedance of electronic devices or energy storage units is relatively low, ranging from several ohms to hundreds of ohm. This mismatch of impedance leads to a very low energy transfer efficiency when directly connecting triboelectric nanogenerators to electronics or energy storage units. Research has focused on designing power management units [8,49] and switches [50–52] to reduce the matching impedance and boost the energy transfer efficiency, however these electronic components increase the complexity and energy consumption of the system [8,53], and are not applicable universally[8], which decelerates the speed of translating these advances to devices [8,49]. Therefore, in addition to developing power management units, there needs to be a focus on addressing the challenge from a materials development perspective. One of the possible approaches is to increase the electrical conductivity of the triboelectric material without sacrificing the triboelectric output, which is complex because electrical conductivity tends to reduce the surface charges created from triboelectrification through leakage effects [54,55]. Previous studies found that adding conductive fillers, such as metal nanoparticles [56–58] and graphite particles [59], into a polymer matrix can enhance the triboelectric output of polymers. However, due to leakage from conductive losses, the amount of the conductive fillers added in these studies has to be below the percolation threshold, generally under 5 wt%, essentially limiting the potential improvement [54,55].

Fortunately, some studies have found that specific conductive fillers, such as carbon nanotubes [60,61] and MXene [62], showed an increase in the triboelectric output even when the filler content reached the percolation threshold, which might be attributed to the large increase in the triboelectric polarity difference between the fillers and the reference material. For example, Rasel et al. [60] found that the triboelectric output of multi-wall carbon nanotube/PDMS composite improved as the weight percent reached 1.5 wt%, which is above the percolation threshold; Wang et al. [62] made a 3D-MXene/ PDMS composite whose electrical conductivity reached 5.5 S/cm, and its triboelectric output was higher than that of pure PDMS. These findings suggest the possibility of increasing electrical conductivity and triboelectric output simultaneously. However, there is often a trade-off between high electrical conductivity and good flexibility in many conductive-filler embedded composites due to the higher volume content of fillers needed [63,64]. This is an issue because flexibility and stretchability are essential for materials that are employed in triboelectric nanogenerators since the major potential applications for triboelectric nanogenerators are wearable electronics. Some studies tried to simplify the structure of the triboelectric nanogenerator and enhance its flexibility by integrating the contacting layer and electrode together. The materials in these studies have a polymer-rich part that acts as the contacting layer, and a conductive filler-rich part that connects with external circuits. For example, Chen et al. [65] fabricated a crumbled-graphene triboelectric nanogenerator with a crumbled-graphene film acting as both the electrode and contacting layer; Pan et al. [64] fabricated a sedimented liquid metal elastomer composite that is ultra-stretchable for triboelectric nanogenerators. Though the structure of the device can be simplified, the polymer-rich part of these material increases the total impedance of the device, which cannot solve the high internal impedance problem of triboelectric nanogenerators. Therefore, developing materials that possess relatively high electrical conductivity, enhanced triboelectric output as well as good mechanical flexibility, although difficult, is potentially transformative for the wide adoption of triboelectric nanogenerators. Employing these materials into triboelectric nanogenerators would address the need for flexibility of electrodes, the impedance matching of the system, and simplify the structure of triboelectric nanogenerators. In addition, systematically investigating the effect of adding fillers on different material properties, such as triboelectric output, electrical conductivity, dielectric permittivity and flexibility, is important for fabricating suitable materials for triboelectric nanogenerators.

This study provides a facile method to simultaneously enhance the flexibility, electrical conductivity, and triboelectric output of polydimethylsiloxane (PDMS). The material properties, surface roughness and triboelectric output of single wall carbon nanotube (SWCNT)-PDMS composites with different SWCNT weight ratios were first investigated to determine a suitable SWCNT content. Then, ionic liquid (IL)-coated SWCNTs were mixed into PDMS matrix without any additional chemical modification. Both the electrical properties and the mechanical properties of the composites were characterized and analyzed. In addition, the triboelectric output of the resulting composites was measured, where both the open-circuit voltage (V_{oc}) and the short-circuit current (I_{sc}) showed an increase compared to pure PDMS. Finally, the mechanism responsible for the change in electrical properties and triboelectric output are proposed and discussed.

2. Material and methods

2.1. Materials

SWCNTs, purchased from US research nanomaterials Inc, were prepared by chemical vapor deposition with a composition of carbon greater than 98%. The diameter of the SWCNTs ranges from 1 to 2 nm and the length ranges from 5 to 30 μm. The electrical conductivity of the SWCNTs is greater than 100 S/cm. The IL, 1-Butyl-3-methylimidazolium Bis(trifluoromethanesulfonyl)imide was purchased from TCI Co., Ltd, and its chemical structure is shown in Fig. S1. The PDMS (Sylgard 184) base and curing agent were purchased from Dow Corning. The solvent for mixing the filler and polymer matrix is toluene, which was obtained from the Science Company. The reference materials, Teflon and Nylon, were purchased from McMaster-Carr Supply Company.

2.2. Preparation of the composites

The material processing steps of the SWCNT-IL-PDMS composites were as follows: as received SWCNTs and different ratio of IL (IL: SWCNT =0:1, 3:1, 10:1, 20:1) were ground with a pestle in a mortar for 5 mins, after which gelation was observed. The SWCNT-IL gel was then dispersed in toluene at 1 mg/mL for 15 mins using probe sonication. At the same time, the PDMS base was magnetic stirred in toluene for 1 hr at 300 rpm. Subsequently, the SWCNT-IL/toluene solution and the PDMS base/toluene solution were mixed by probe sonication for 25 mins. The PDMS curing agent (PDMS base: curing agent = 10:1) was then added and the solution was probe-sonicated for another 5 mins, after which the mixture was poured into a petri dish. The petri dish was placed in the fume hood for 2 hrs to evaporate excess toluene, then in an oven at 100℃ for 35 mins to cure the PDMS composite. Finally, the cured composite was vacuumed for 6 hrs at 21℃ to ensure there is no solvent left in the sample. SWCNT-PDMS composites at different SWCNT contents, 0 wt%, 0.01 wt%, 0.1 wt% and 1 wt% (0 vol%, 0.0045 vol%, 0.045 vol% and 0.45 vol% in volume), were fabricated using the same procedure, except that there was no grinding step in the SWCNT-PDMS fabrication process.

2.3. Fabrication of samples for triboelectric experiment

The material pair for the triboelectric experiment consists of a composite material and a reference material. The composite material was cut from the aforementioned composite with a dimension of 2 cm × 3 cm and was attached to a copper tape which serves as the

electrode. The reference material, Teflon or Nylon, was also cut into 2 cm × 3 cm and was attached to a copper tape. Each of the two electrodes was connected to the external circuit with a copper wire. A custom designed set-up, shown in Fig. S2, was used to provide the contact/separation motion. The reference material was attached to the stationary plate of the device and the composite material was attached to the moving plate.

2.4. Experimental characterization

The capacitance and admittance of the materials were characterized with ModuLab XM MTS system from 0.1 Hz to 1 MHz with a 1 V applied AC voltage. The dielectric permittivity, dielectric loss and electrical conductivity of the materials were calculated based on the measured capacitance and admittance. The surface roughness of the samples was measured on a Nexview 3D optical profiler, where the scanned area is about 836μm by 836μm. The tensile and compression testing were done on an MTS testing machine with a 50 N load cell at a crosshead speed of 0.1 mm/s. Imaging of the cross-section of the composites was done with a Verios G4 scanning electron microscope; the cross-section of the composites was freeze-fractured in liquid nitrogen and then sputtered with a layer of iridium. The output voltage of the triboelectric nanogenerator was measured via an electrometer (Keithley 6517 A) and the output current was measured by a picoammeter (Keithley 6487). All the voltage and current data presented here were the peak-to-peak value and were measured at 10 mins after the two triboelectric materials first came into contact.

3. Results and discussion

3.1. SWCNT-PDMS without IL

Different volume percent of SWCNT without IL were mixed into PDMS matrix first to assess the effect of SWCNT on the electrical properties and triboelectric output of the composite. The electrical conductivity and dielectric constant of the composites were measured as a function of frequency and the complete spectra are shared in the supporting information (see Figs. S3 and S4 respectively). According to the percolation theory, a sudden transition from insulator to conductor is observed at the so-called percolation threshold in a mixture of conducting and nonconducting components [66]. The percolation threshold can be calculated using the power law equation below:

$$\sigma_c = \sigma_0 (V_f - V_c)^t$$

Where σ_c is the composite electrical conductivity (S/m); σ_0 is the electrical conductivity of the conductive filler (S/m); V_f is the volume fraction of the filler; V_c is the percolation threshold, and t is the critical exponent. The electrical conductivity of different composites at 1 Hz are plotted as a function of SWCNT's volume percent (Fig. 1). The electrical conductivity of SWCNT σ_0 is set to be around 10,000 S/m according to supplier's datasheet. Using the equation above, the percolation threshold is calculated to be around 0.015 vol% (0.033 wt%), the critical exponent t is 1.92, and the accuracy of fitting is confirmed by $R^2 = 0.98$. Since the percolation threshold of SWCNT/ polymer composites is influenced by several factors, including the aspect ratio, dispersion, and alignment of SWCNTs, there are different reported percolation threshold values. Our calculated value falls in the range of reported percolation threshold for SWCNT/ polymer composites which spans from 0.005 vol% to several vol% [67].

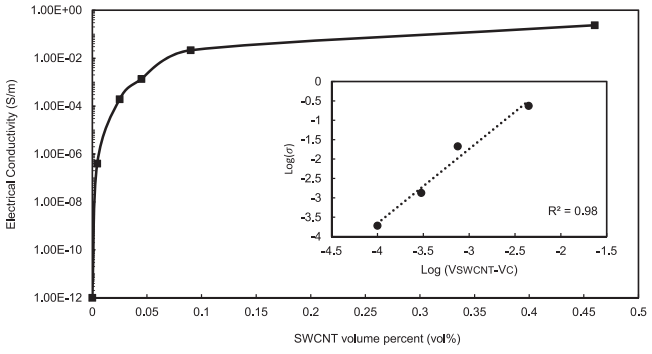

Fig. 1. The electrical conductivity of the composites at 1 Hz as a function of the volume percent of SWCNT. The insert shows a log-log plot of the electrical conductivity as a function of volume fraction – critical volume fraction.

Three composites with different SWCNT content, i.e., 0.01 wt%, 0.1 wt% and 1 wt% (0.0045 vol%, 0.045 vol% and 0.45 vol% in volume), were contacted with reference materials to determine the SWCNT ratio that has the highest triboelectric output. This SWCNT content will then be used in SWCNT-IL-PDMS composites to investigate the effect of IL on the material properties and triboelectric output. Since previous studies showed that the triboelectric polarity of composites might change with the addition of fillers [61,68], two reference materials, Teflon and Nylon, were chosen to contact with the composites, where Teflon has a negative triboelectric polarity while Nylon has a positive one. The two reference materials will ensure that the possible variance in the triboelectric output caused by change in the triboelectric polarity can be eliminated. The average value of measured open-circuit voltage of the composites with respect to Nylon and Teflon are shown in Fig. 2 (a), and the data of all four measurements for each material pair are shown in Fig. S5. From Fig. 2(a), the triboelectric output increased with increasing SWCNT weight percent until the weight ratio reached 0.1 wt % for both reference materials. Specifically, the average V_{oc} increased from 18 V to 23 V when the composites contacted with Nylon and the average V_{oc} increased from 19 V to 42 V when contacted with Teflon. This enhancement in triboelectric output is a result of the increase in dielectric permittivity, which increased from 4.4 (0.01 wt%) to 58 (0.1 wt%). The triboelectric output then decreased when the SWCNT content was further increased to 1 wt%; the average V_{oc} when the reference material was Nylon decreased to 5 V, and when the reference material was Teflon to 30 V. This decrease is because adding SWCNTs into PDMS matrix increases both the dielectric permittivity and the electrical conductivity of the composites, resulting in a competition between both. First, the increase in dielectric permittivity dominates the triboelectric mechanism, however, at the higher content, the increase in electrical conductivity is such that the triboelectric output starts to decrease due to leakage of surface charges, indicating that there is an optimum SWCNT ratio that yields the highest triboelectric output.

In addition to the trade-off between dielectric permittivity and electrical conductivity, other factors might also affect the triboelectric output. From Fig. 2(a), though the general trend for V_{oc} is the same for both reference materials, a difference in the relative V_{oc} magnitude of the 1 wt% SWCNT-PDMS compared with the V_{oc} magnitude of pure PDMS in the two plots is observed. The average V_{oc} of the 1 wt% SWCNT-PDMS contacting with Nylon is 5 V, which is lower than the average V_{oc} of pure PDMS contacting with Nylon (18 V). When the reference material is Teflon, the average V_{oc} of 1 wt% SWCNT-PDMS, which is 29 V, is higher than that of pure PDMS (19 V). It is surmised that, because SWCNT is more triboelectrically positive than PDMS [61, 68], the triboelectric polarity of the SWCNT-PDMS composite shifts to the more positive side when the weight percent of SWCNT reaches 1 wt %. Therefore, the triboelectric polarity difference between 1 wt% SWCNT-PDMS and Nylon is smaller than the PDMS and Nylon pair, which results in a lower total amount of triboelectric charges generated on the contacting surfaces of the 1 wt% SWCNT-PDMS and Nylon pair. This argument can be further demonstrated by investigating the surface roughness of the SWCNT-PDMS samples.

The surface roughness of the three SWCNT-PDMS samples and pure PDMS were measured to monitor the change in surface roughness with the addition of fillers. Since the materials were prepared in petri-dishes,

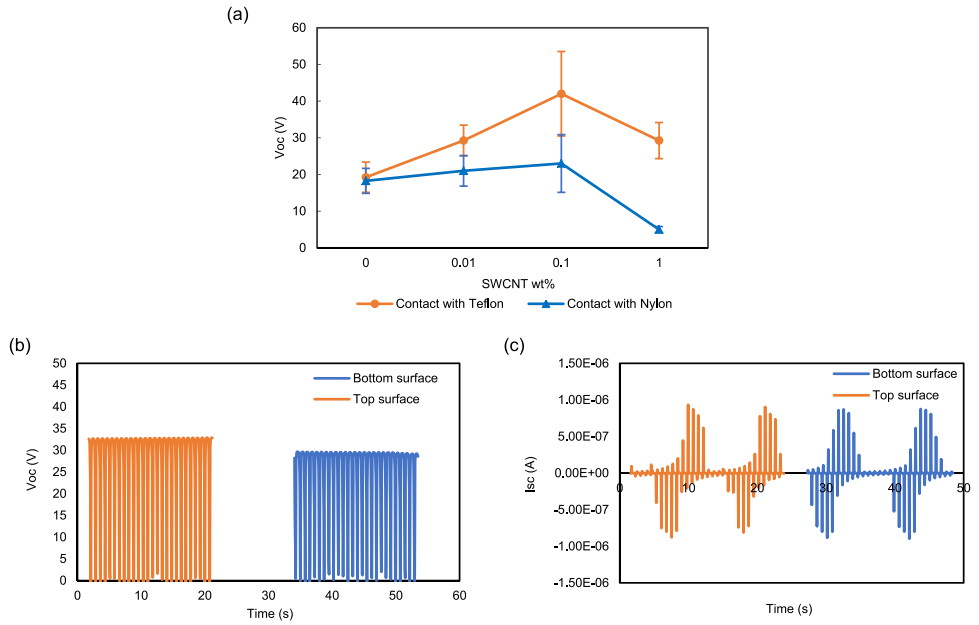

Fig. 2. (a) The average open-circuit voltage of SWCNT-PDMS composite with different weight percent of SWCNT contacting with Nylon and Teflon respectively. Error bars represent standard deviation. (b) The open-circuit voltage and (c) the short-circuit current of the 1 wt% SWCNT-PDMS sample with the bottom surface and the top surface contacting with Teflon respectively.

the surface roughness of the surface contacting the petri-dish (bottom surface) and the surface exposed to air (top surface) are different. Therefore, the surface roughness of both the top and bottom surfaces were measured and the root mean square (RMS) values are listed in Table 1, while the optical profilometry images are shown in Fig. S6. Both the top and bottom surface roughness values increase with increasing SWCNT content, and the surface roughness begins to experience a large increase when the SWCNT weight percent reaches 0.1 wt% (Table 1). In particular, for the 1 wt% SWCNT-PDMS composite, the top surface roughness is 3.5-folds higher than the 0.1 wt% sample and the bottom surface roughness is 2.4-fold higher. This large increase in surface roughness supports the argument that the triboelectric polarity might change for the 1 wt% SWCNT-PDMS composite; the high surface roughness indicates that some of the SWCNTs might be located near the surface, which could change the triboelectric polarity of the composite from a value closer to the triboelectric polarity of PDMS to one closer to the triboelectric polarity of SWCNT. It is worth noting that though the addition of fillers increases the average value of surface roughness, it cannot produce well-ordered microstructures, which increases the standard deviation of the surface roughness, i.e., a less consistent height profile, and thus decreases the real contact area and triboelectric output [69]. Moreover, for the pure PDMS and 0.01 wt% SWCNT-PDMS composite, there is not much difference between the top and bottom surface roughness, while the top surface of the 0.1 wt% and 1 wt% SWCNT-PDMS composite is much rougher than the bottom surface. In order to examine whether the difference in the surface roughness of the top and bottom surfaces affects the triboelectric output, the V_{oc} and I_{sc} of the 1 wt% SWCNT-PDMS sample were measured with the bottom surface and the top surface contacting with Teflon respectively, which are shown in Fig. 2(b)-(c). From the figure it can be seen that the change in the triboelectric output is small, specifically, the V_{oc} only decreased 3 V when changing from top surface to bottom surface. Therefore, the surface roughness of the top and bottom surfaces has little effect on the triboelectric output of the sample, and its influence is on the triboelectric polarity as surmised.

Table 1
Surface roughness of the top and bottom surface of pure PDMS and SWCNT-PDMS samples.

SWCNT weight percent (%)	Surface RMS roughness (μm)	
	top	bottom
0	0.011	0.008
0.01	0.061	0.053
0.1	1.398	0.15
1	4.848	0.362

In summary, the 0.1 wt% SWCNT-PDMS has the highest triboelectric output, therefore it is used for further investigation on the effect of adding ionic liquid on the triboelectric output. Furthermore, this part of the study shows that, since the working mechanism of triboelectric nanogenerator is a combination of triboelectric effect and electrostatic induction [70], the output voltage is enhanced either by increasing the triboelectric polarity difference between the two contacting surfaces to increase the number of charges generated by triboelectric effect, or by increasing the dielectric constant to increase the capacitance. The reduction of the output voltage caused by the increased electrical conductivity can be compensated by increasing the triboelectric polarity difference between the two contacting surfaces.

3.2. SWCNT-PDMS with IL

As discussed in the previous section, the triboelectric output and electrical conductivity of the SWCNT-PDMS composite can be simultaneously increased by tuning the SWCNT ratio. Specifically, the 0.1 wt% (0.045 vol%) SWCNT-PDMS and Teflon pair has the largest triboelectric output, and the electrical conductivity of 0.1 wt% SWCNT-PDMS (above the percolation threshold) reaches a value of 0.0013 S/m. Therefore, the 0.1 wt% SWCNT-PDMS can serve both as the contacting material and the electrode of the triboelectric nanogenerator. In order to make the composite applicable to wearable devices, having a good flexibility is another criterion for the composite. The flexibility of the material can be quantified by the elastic modulus, i.e., the material is more flexible when the elastic modulus is lower. Ideally, the materials that are designated for wearable devices should have a “skin-like” feeling, which means that the elastic modulus of the material should be comparable to that of the human skin (10–500 kPa) [71,72]. The elastic modulus of the 0.1 wt% SWCNT-PDMS was measured to be 1.83 MPa, which is not desirable for wearable devices. Therefore, in order to enhance the flexibility of the

composite while maintaining or even increasing the triboelectric output and electrical conductivity, different amounts of IL were added to the 0.1 wt% SWCNT-PDMS. The IL to SWCNT ratio was set to 0:1, 3:1, 10:1 and 20:1, respectively.

The average dielectric constant and electrical conductivity of SWCNT-IL-PDMS samples with different IL: SWCNT ratio over a range of frequencies are illustrated in Fig. 3, and the original data is plotted in Fig. S7. From Fig. 3, the 3:1 sample has the highest dielectric constant and electrical conductivity while the sample without IL (0:1) has the lowest electrical properties. Specifically, the dielectric constant of the 3:1 sample is about 4 times higher than that of the sample without ionic liquid, and the electrical conductivity is 10 times higher than that of the sample without ionic liquid at 0.1 MHz. This increase in the dielectric constant and electrical conductivity is possibly due to the better dispersion of SWCNT in the polymer matrix[73–79]; the interaction between ionic liquid and SWCNT after grinding hinders the "$\pi - \pi$" stacking between SWCNTs, which can prevent the aggregation of SWCNTs and form an interconnected network structure. The decrease of the electrical properties with a further addition of IL might because of the formation of ion pairs. The ions will be very close to each other after the IL reaches a certain value which forms ion clusters and restrains the mobility of ions. The SWCNT might be trapped into the ion clusters which adds to the decrease of electrical properties. This can be verified with the SEM images (Fig. 4). Little to no ion clusters are observed in the 3:1 sample (Fig. 4(b)), while some ion clusters appeared in the 10:1 sample (Fig. 4(c)). The ion clusters became larger in the 20:1 sample when compared to the 10:1 sample. In addition, SWCNT agglomeration is seen in the sample without IL, which is shown in the insert in 4(a), while no large SWCNT agglomeration was discovered in the samples with IL. Also, some SWCNTs are trapped in the ion clusters in the 20:1 sample as shown in the insert in 4(d).

To examine the flexibility of the composite, both compressive stress and tensile stress were measured with an increasing strain, where five samples were tested for each IL: SWCNT ratio; the data is shown in Fig. S8. Selected stress-strain plots for each ratio are shown in Fig. 5 and the corresponding elastic modulus up to 2% and 10% strain for compressive and tensile testing respectively are summarized in Table 2. Both the tensile and compressive elastic modulus decreased with increasing IL content. The tensile elastic modulus of the 20:1 sample is less than half of that of the sample without IL. The decrease of the compressive elastic modulus is not as significant as the tensile elastic modulus but the compressive elastic modulus of the 20:1 sample is still decreased to 60% of that of the sample without IL. In addition, the tensile stress-strain plot until break is shown in Fig. S9, the strain at break of the 20:1 sample reached to 158%, which is higher than other samples, so the 20:1 sample has the best flexibility and ductility. The decrease in elastic modulus is due to the fact that IL can act as plasticizer in PDMS matrix, which is consistent with the findings in the literature [73,76]. Moreover, the ion clusters in the samples with higher IL to SWCNT ratio are stable and can sustain large applied strains by either tension or compression. The elastic modulus can be further decreased by increasing the IL: SWCNT ratio which can potentially meet the requirement for wearable devices.

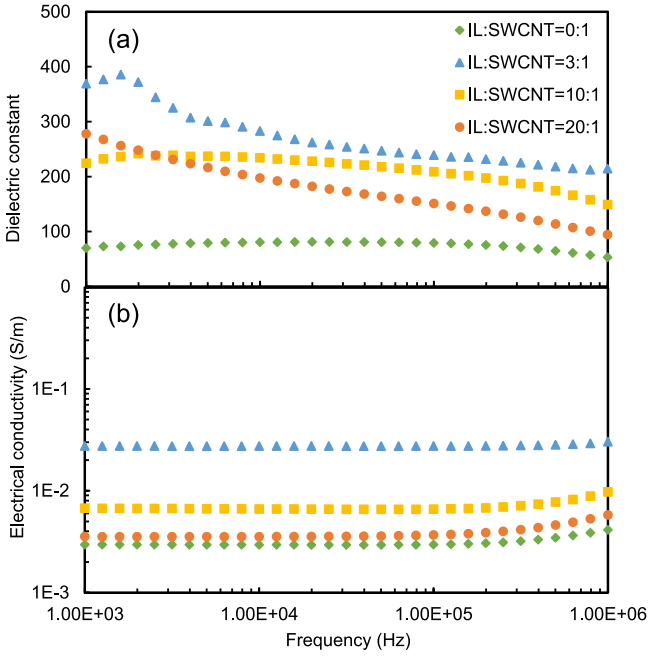

Fig. 3. The average (a) dielectric constant and (b) electrical conductivity of the SWCNT-IL-PDMS composite with an IL to SWCNT ratio of 0:1, 3:1, 10:1 and 20:1, respectively.

The samples with different IL to SWCNT ratio were contacted with Teflon several times, and the measured V_{oc} and I_{sc} are shown in Fig. S10. The average values of the V_{oc} and I_{sc} are shown in Fig. 6(a). From Fig. 6 (a), both the average voltage and current of the samples with IL increased comparing to 0.1 wt% SWCNT-PDMS. Interestingly, the triboelectric output of the 20:1 sample is higher than the 3:1 sample while the dielectric constant of the 20:1 sample is lower than the 3:1 sample. As discussed earlier, this enhancement in the triboelectric output of the 20:1 sample is likely due to (1) the trade-off between high dielectric constant and high electrical conductivity of the 3:1 sample, and (2) the shifting of triboelectric polarity with the addition of IL. The shifting of triboelectric polarity of the composites with IL can be verified by contacting with Nylon. From Fig. 6(b), the V_{oc} changed from negative to positive when there is IL in the composite, which means that the composites with IL are even more triboelectrically positive than Nylon. The shifting of the triboelectric polarity to the more positive side might result from the N^+ and N^- in the cation and anion of IL, (see Fig. S1 for IL structure). A previous study indicated that nitrogen containing polymers are most likely to be triboelectrically positive [80], further reinforcing that the triboelectric polarity of the SWCNT-IL-PDMS composites became more positive compared to the SWCNT-PDMS composite. The existence of Nitrogen in the SWCNT-IL-PDMS composite was detected by ATR-FTIR spectroscopy, and the spectra of PDMS and SWCNT-IL-PDMS are shown in Fig. 7. The SWCNT-IL-PDMS sample can be distinguished from the control PDMS by several characteristic peaks of the IL. In particular, the peak at 1050 cm^{-1} represents the S-N-S asymmetric stretching and the NCH_3 twisting [77,81], which confirms that nitrogen exists near the surface of the composite.

From previous discussion, the 20:1 sample has a good flexibility and an enhanced triboelectric output compared with pure PDMS. However, in order to conclude that the composite can serve as both the flexible electrode and the contacting layer, the electrical conductivity of the composite has to be high enough such that the charges can be directly transferred to the external circuit. Therefore, the triboelectric output of the 20:1 sample without an electrode was measured to verify the composite's ability to transfer charges. The 20:1 sample was attached to an electrode and contacted with a Teflon film at first, immediately after which the same 20:1 sample was contacted with the same Teflon without an electrode. The V_{oc} and I_{sc} of the 20:1 sample, with and without an electrode, contacting with Teflon are plotted in Fig. S11 respectively. The V_{oc} of the composite without electrode reached to 62 V while the same sample with electrode was measured to be 72 V; the I_{sc} of the sample with and without electrode were 2.06 μA and 1.92 μA respectively. The voltage decreased by 14% and the current decreased by 7%. Although both the voltage and current of the composite without an electrode were smaller than the composite with an electrode, the decrease of the triboelectric output is acceptable. In addition, the durability of the 20:1 sample was tested by contacting with Teflon for 20,000 cycles continuously, which lasted for a total of 4.3 hrs. The measured V_{oc} (at every 400 cycles) is shown in Fig. 6(c). The V_{oc} fluctuated between 83 V and 86 V, and did not show a significant decrease

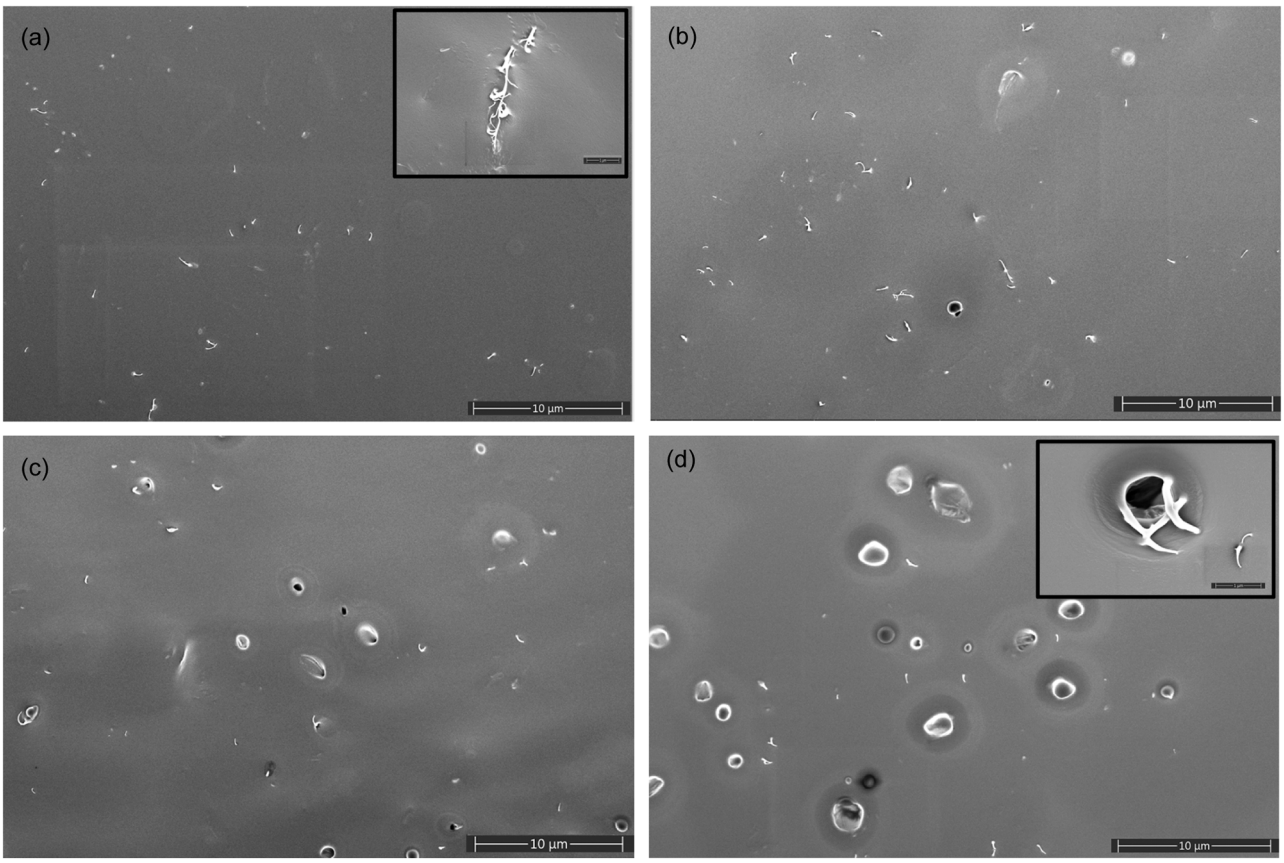

Fig. 4. SEM images of SWCNT-IL-PDMS composites with a (a) 0:1, (b) 3:1, (c) 10:1 and (d) 20:1 IL to SWCNT ratio. The insert in (a) shows the SWCNT agglomeration in the 0:1 sample and the insert in (d) indicates that the SWCNTs are trapped in an ion cluster in the 20:1 sample. The scale bar in the inserts is 1 μm.

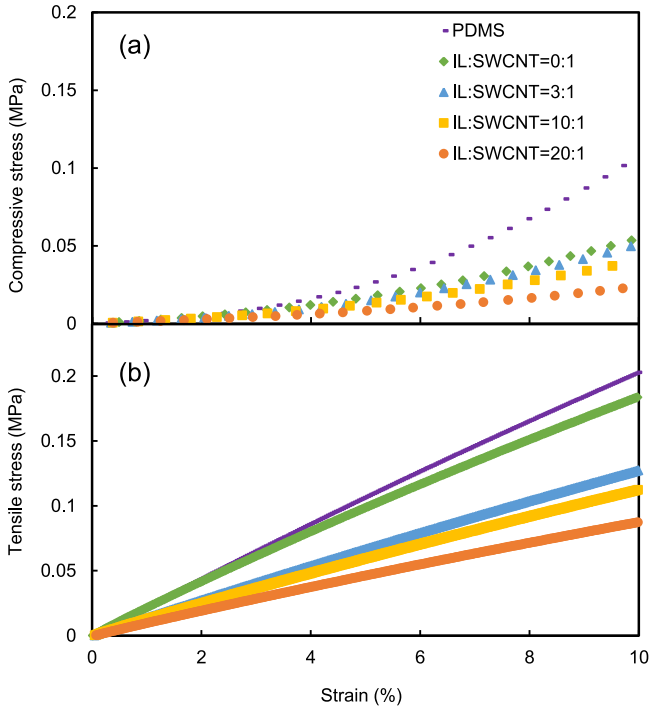

Fig. 5. (a) The compressive stress and (b) the tensile stress as a function of strain for PDMS, 0.1 wt% SWCNT-IL-PDMS with IL: SWCNT ratio of 0:1, 3:1, 10:1 and 20:1, respectively.

Table 2
The tensile and compressive elastic modulus for PDMS and SWCNT-IL-PDMS composites.

IL: SWCNT	PDMS	0:1	3:1	10:1	20:1
Tensile E @ 10% strain (MPa)	2.02	1.83	1.27	1.15	0.83
Compressive E @ 2% strain (MPa)	0.27	0.23	0.19	0.17	0.14

after the 20,000 cycles, which demonstrates the excellent output durability of the sample. Moreover, the effect of humidity on the triboelectric output of the samples was examined at two different humidity ranges, and the corresponding V_{oc} is listed in Table S1. From the table, it can be seen that all the samples generated a larger V_{oc} in a lower humidity environment. Specifically, the V_{oc} of pure PDMS decreased by 27% and that of the 20:1 sample decreased by 45% when the humidity increased about twofold. Though the decrease for the 20:1 sample is higher than that of the pure PDMS, the V_{oc} of the 20:1 sample is still two-times higher than that of pure PDMS.

Another outcome of the increase of the electrical conductivity that needs to be examined is the ability to decrease the internal impedance of the triboelectric nanogenerator. The internal impedance of the triboelectric nanogenerator is quantified by measuring the optimum matching external resistance, i.e., the external resistance yields the highest power, of the composite contacting with Teflon. The voltage and current across different external resistances were measured and the corresponding power were calculated. The voltage, current and power for PDMS and the 20:1 sample contacting with Teflon are plotted as a function of resistance and shown in Fig. 8. From the figure, the optimum matching resistance of the 20:1 sample is around 180 MΩ which is about 42% of the pure PDMS (430 MΩ). The corresponding maximum power of the 20:1 sample and Teflon is 72μW, which is 7 folds higher than the

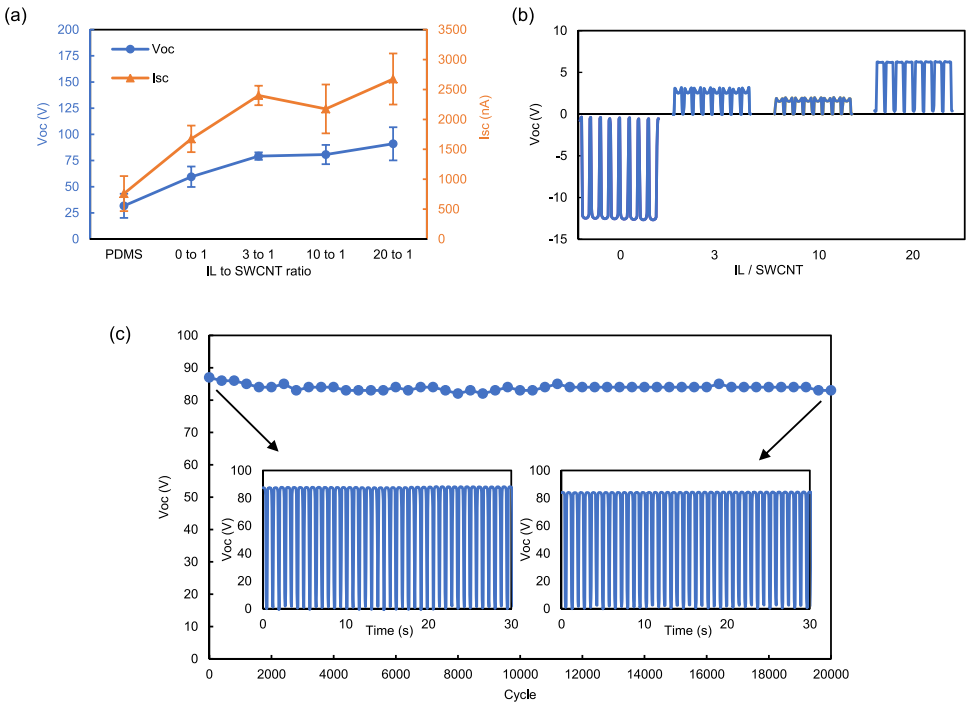

Fig. 6. (a) The average open-circuit voltage and short-circuit current of PDMS and SWCNT-IL-PDMS composite with different IL to SWCNT ratio contacting with Teflon. Error bars represent standard deviation. (b) The V_{oc} plot of SWCNT-IL-PDMS composite with different IL to SWCNT ratio contacting with Nylon. (c) Durability assessment of the 0.1 wt% SWCNT-IL-PDMS (IL: SWCNT= 20: 1) sample over 20,000 cycles. The left and right inserts are the V_{oc} plot from the 1st cycle and the 20,000th cycle respectively.

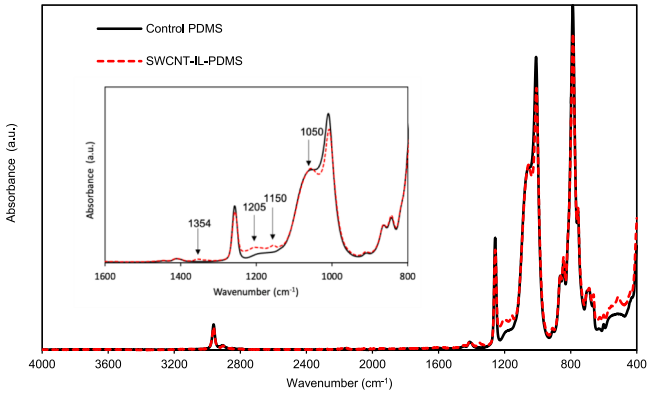

Fig. 7. ATR-FTIR spectra of the 0.1 wt% SWCNT-IL-PDMS (IL: SWCNT= 20: 1) sample and the PDMS control sample. The insert shows the characteristic peaks of the 0.1 wt% SWCNT-IL-PDMS (IL: SWCNT= 20: 1) sample in the wavenumber range between 800 cm^{-1} and 1600 cm^{-1}.

pure PDMS and Teflon pair. Though the reduction of the impedance is not large enough for practical uses, it showed the feasibility of tuning the impedance of triboelectric nanogenerators by changing the material's electrical properties. Therefore, the ionic liquid/single-wall carbon nanotube/PDMS composite can be employed in triboelectric nanogenerators to potentially solve the flexibility problem of electrodes, the impedance matching problem of the system, and simplify the structure of triboelectric nanogenerators.

Recent experimental studies on PDMS composites that reported both the change in electrical conductivity or resistance and the change in triboelectric output are summarized in Table 3. Since the value of the triboelectric output is dependent on the applied force, surface area and reference material, and since that information is not readily available from the publications, it is more meaningful to compare the percent increase. The electrical conductivity of our work increased by 10 orders of magnitude, the open-circuit voltage (V_{oc}) and the short-circuit current (I_{sc}) increased 200% and 234% respectively. From the table, the enhancement in electrical conductivity and triboelectric output of this work compares well with other reported PDMS composites. Though the increased ratio of the AgNWs-PDMS [82] is slightly higher than our work, the areal factor of AgNWs to PDMS has reached to 0.59:0.41 which means the amount of added AgNWs is large and might decrease the flexibility and stretchability of PDMS. In summary, the SWCNT-IL-PDMS composite possess relatively high electrical conductivity, enhanced triboelectric output as well as good flexibility, which is essential for triboelectric nanogenerators.

4. Conclusions

In conclusion, a flexible and electrically conductive SWCNT-IL-PDMS

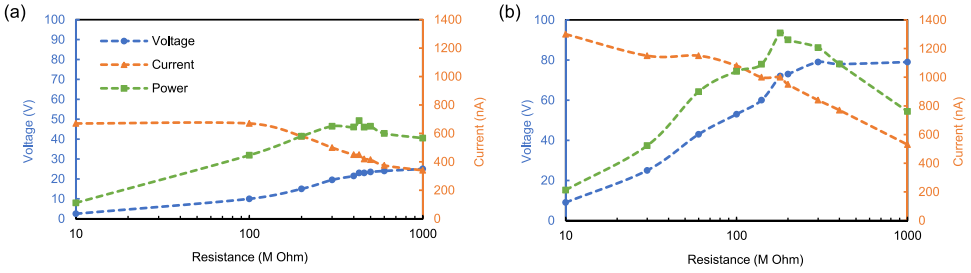

Fig. 8. The voltage, current and power across different external resistances for (a) pure PDMS and (b) 0.1 wt% SWCNT-IL-PDMS composite (IL: SWCNT=20:1) contacting with Teflon, respectively.

Table 3
Comparison of the enhancement in electrical conductivity and triboelectric output of different PDMS composites.

Polymer matrix	Filler	Reference material	Filler content	Resistance/Electrical conductivity	Current	Voltage	Ref.
PDMS	Aligned CNT	PDMS	NA	Sheet resistance decreased from 4.5kΩ/sq to 0.28kΩ/sq	NA	Increased from 90 V to 150 V (Increased 67%)	[61]
PDMS	3D-MXene (Ti_3C_2Tx)	Nylon	Increased from 0 to 2.5 vol%	Conductivity increased from 10^{-14} S/cm to 5.5 S/cm	Increased from ~0.2 μA to ~0.6 μA (Increased 200%)	Increased from 33 V to 45 V (Increased 36%)	[62]
PDMS	AgNWs	PFA	Areal factor increased from 0.18 to 0.59	Sheet resistance decreased from 406 Ω/sq to 5 Ω/sq	Increased from ~6 μA to ~22 μA (Increased 267%)	Increased from ~30 V to ~128 V (Increased 327%)	[82]
PDMS	SWCNT and IL	Teflon	0.1 wt% SWCNT + IL (increased from 0 to 2 wt%)	Conductivity increased from 10^{-13} S/m to 0.004 S/m	Increased from ~0.8 μA to ~2.5 μA (Increased 212%)	Increased from ~30 V to ~90 V (Increased 200%)	Current work

composite with enhanced triboelectric performance was fabricated. The composite achieved a relatively high electrical conductivity that enables the transfer of charges without the need for additional electrodes, which is seen as positive since it leads to a reduction of the internal impedance of triboelectric nanogenerators. The enhancement of the flexibility was demonstrated by the reduction of the tensile and compressive elastic moduli. Moreover, the open-circuit voltage (V_{oc}) and the short-circuit current (I_{sc}) are 3-fold higher than that of pure PDMS. Therefore, the SWCNT-IL-PDMS composite can be potentially employed in triboelectric nanogenerators, especially ones for powering wearable electronics, since this composite strategy addresses the flexibility issue of electrodes, the impedance matching issue of the system, and it results in a simplified overall structure of the triboelectric nanogenerators. In addition, the approaches to increase the output voltage are experimentally correlated to either (a) the increase of the triboelectric polarity difference between the two contacting surfaces where the number of charges generated by triboelectric effect is enhanced, or (b) increase of the dielectric constant to increase the capacitance. Finally, we demonstrate that the reduction of the output voltage caused by increased electrical conductivity could be compensated by increasing the triboelectric polarity difference between the two contacting surfaces. This study generalizes the approach for increasing the triboelectric output and paves the way to explore new flexible and electrically conductive materials for wearable triboelectric nanogenerators.

CRediT authorship contribution statement

Xiaoyue Zhao: Conceptualization, Data curation, Formal analysis, Investigation, Writing – original draft. **Zoubeida Ounaies**: Funding acquisition, Methodology, Project administration, Resources, Software, Supervision, Roles/Writing – original draft, Writing – review & editing.

Declaration of Competing Interest

The authors declare that they have no known competing financial interests or personal relationships that could have appeared to influence the work reported in this paper.

Acknowledgments

The authors would like to acknowledge support from the Penn State Convergence Center for Living Multifunctional Material Systems (LiMC^2). In addition, XZ was partially funded by NSF DMREF 1921969.

Appendix A. Supporting information

Supplementary data associated with this article can be found in the online version at doi:10.1016/j.nanoen.2021.106908.

References

[1] Z.L. Wang, Entropy theory of distributed energy for internet of things, Nano Energy 21 (2019), https://doi.org/10.1016/j.nanoen.2019.02.012.
[2] A. Ahmed, I. Hassan, M.F. El-Kady, A. Radhi, C.K. Jeong, P.R. Selvaganapathy, J. Zu, S. Ren, Q. Wang, R.B. Kaner, Integrated triboelectric nanogenerators in the era of the internet of things, Adv. Sci. 6 (2019), 1802230, https://doi.org/10.1002/advs.201802230.
[3] R.D.I.G. Dharmasena, S.R.P. Silva, Towards optimized triboelectric nanogenerators, Nano Energy 62 (2019) 530–549, https://doi.org/10.1016/j.nanoen.2019.05.057.
[4] Z.L. Wang, On Maxwell's displacement current for energy and sensors: the origin of nanogenerators, Mater. Today 20 (2017) 74–82, https://doi.org/10.1016/j.mattod.2016.12.001.
[5] C. Wu, A.C. Wang, W. Ding, H. Guo, Z.L. Wang, Triboelectric nanogenerator: a foundation of the energy for the new era, Adv. Energy Mater. 9 (2019) 1–25, https://doi.org/10.1002/aenm.201802906.
[6] G. Bedi, G.K. Venayagamoorthy, R. Singh, R.R. Brooks, K.C. Wang, Review of Internet of Things (IoT) in electric power and energy systems, IEEE Internet Things J. 5 (2018) 847–870, https://doi.org/10.1109/JIOT.2018.2802704.
[7] S. Niu, Z.L. Wang, Theoretical systems of triboelectric nanogenerators, Nano Energy 14 (2014) 161–192, https://doi.org/10.1016/j.nanoen.2014.11.034.
[8] X. Cheng, W. Tang, Y. Song, H. Chen, H. Zhang, Z.L. Wang, Power management and effective energy storage of pulsed output from triboelectric nanogenerator, Nano Energy 61 (2019) 517–532, https://doi.org/10.1016/j.nanoen.2019.04.096.
[9] Y. Zhou, W. Deng, J. Xu, J. Chen, Engineering materials at the nanoscale for triboelectric nanogenerators, Cell Rep. Phys. Sci. 1 (2020), 100142, https://doi.org/10.1016/j.xcrp.2020.100142.
[10] F. Yi, Z. Zhang, Z. Kang, Q. Liao, Y. Zhang, Recent advances in triboelectric nanogenerator-based health monitoring, Adv. Funct. Mater. 29 (2019), https://doi.org/10.1002/adfm.201808849.
[11] Y. Zou, J. Xu, Y. Fang, X. Zhao, Y. Zhou, J. Chen, Nano Energy Full paper A hand-driven portable triboelectric nanogenerator using whirligig spinning dynamics, Nano Energy 83 (2021), 105845, https://doi.org/10.1016/j.nanoen.2021.105845.
[12] X. Shi, S. Zhang, S. Gong, A self-powered and arch-structured triboelectric nanogenerator for portable electronics and human-machine communication, J. Mater. Chem. A. 8 (2020) 8997–9005, https://doi.org/10.1039/d0ta02178d.
[13] Y. Zi, H. Guo, Z. Wen, M.H. Yeh, C. Hu, Z.L. Wang, Harvesting Low-Frequency (<5 Hz) Irregular Mechanical Energy: A Possible Killer Application of Triboelectric Nanogenerator, ACS Nano 10 (2016) 4797–4805, https://doi.org/10.1021/acsnano.6b01569.
[14] Z.L. Wang, T. Jiang, L. Xu, Toward the blue energy dream by triboelectric nanogenerator networks, Nano Energy (2017), https://doi.org/10.1016/j.nanoen.2017.06.035.
[15] T.C. Hou, Y. Yang, H. Zhang, J. Chen, L.J. Chen, Z. Lin Wang, Triboelectric nanogenerator built inside shoe insole for harvesting walking energy, Nano Energy 2 (2013) 856–862, https://doi.org/10.1016/j.nanoen.2013.03.001.
[16] W. Yang, J. Chen, G. Zhu, J. Yang, P. Bai, Y. Su, Q. Jing, X. Cao, Z.L. Wang, Harvesting energy from the natural vibration of human walking, ACS Nano 13 (2013) 847–853, https://doi.org/10.1021/nn405175z.
[17] T. Huang, C. Wang, H. Yu, H. Wang, Q. Zhang, M. Zhu, Human walking-driven wearable all-fiber triboelectric nanogenerator containing electrospun polyvinylidene fluoride piezoelectric nanofibers, Nano Energy (2014), https://doi.org/10.1016/j.nanoen.2015.01.038.
[18] F. Xing, Y. Jie, X. Cao, T. Li, N. Wang, Natural triboelectric nanogenerator based on soles for harvesting low-frequency walking energy, Nano Energy 42 (2017) 138–142, https://doi.org/10.1016/j.nanoen.2017.10.029.
[19] P. Vasandani, B. Gattu, J. Wu, Z.H. Mao, W. Jia, M. Sun, Triboelectric Nanogenerator Using Microdome-Patterned PDMS as a Wearable Respiratory Energy Harvester, Adv. Mater. Technol. 2 (2017) 1–9, https://doi.org/10.1002/admt.201700014.
[20] Y. Su, G. Chen, C. Chen, Q. Gong, G. Xie, M. Yao, H. Tai, Y. Jiang, J. Chen, Self-powered respiration monitoring enabled by a triboelectric nanogenerator, Adv. Mater. 33 (2021), 2101262, https://doi.org/10.1002/adma.202101262.

[21] S. Wang, H. Tai, B. Liu, Z. Duan, Z. Yuan, H. Pan, Y. Su, G. Xie, X. Du, Y. Jiang, A facile respiration-driven triboelectric nanogenerator for multifunctional respiratory monitoring, Nano Energy (2019), https://doi.org/10.1016/j.nanoen.2019.01.042.
[22] J. Chen, G. Zhu, W. Yang, Q. Jing, P. Bai, Y. Yang, T.C. Hou, Z.L. Wang, Harmonic-resonator-based triboelectric nanogenerator as a sustainable power source and a self-powered active vibration sensor, Adv. Mater. 25 (2013) 6094–6099, https://doi.org/10.1002/adma.201302397.
[23] W. Yang, J. Chen, G. Zhu, X. Wen, P. Bai, Y. Su, Y. Lin, Z. Wang, Harvesting vibration energy by a triple-cantilever based triboelectric nanogenerator, Nano Res 6 (2013) 880–886, https://doi.org/10.1007/s12274-013-0364-0.
[24] M. Xu, P. Wang, Y.C. Wang, S.L. Zhang, A.C. Wang, C. Zhang, Z. Wang, X. Pan, Z. L. Wang, A soft and robust spring based triboelectric nanogenerator for harvesting arbitrary directional vibration energy and self-powered vibration sensing, Adv. Energy Mater. (2018), https://doi.org/10.1002/aenm.201702432.
[25] H. Zhang, Y. Yang, X. Zhong, Y. Su, Y. Zhou, C. Hu, Z.L. Wang, Single-electrode-based rotating triboelectric nanogenerator for harvesting energy from tires, ACS Nano (2014), https://doi.org/10.1021/nn4053292.
[26] T. Guo, G. Liu, Y. Pang, B. Wu, F. Xi, J. Zhao, T. Bu, X. Fu, X. Li, C. Zhang, Z. L. Wang, Compressible hexagonal-structured triboelectric nanogenerators for harvesting tire rotation energy, Extrem. Mech. Lett. 18 (2018) 1–8, https://doi.org/10.1016/j.eml.2017.10.002.
[27] Y. Mao, D. Geng, E. Liang, X. Wang, Single-electrode triboelectric nanogenerator for scavenging friction energy from rolling tires, Nano Energy 21 (2015) 610–616, https://doi.org/10.1016/j.nanoen.2015.04.026.
[28] Y. Yang, G. Zhu, H. Zhang, J. Chen, X. Zhong, Z.H. Lin, Y. Su, P. Bai, X. Wen, Z. L. Wang, Triboelectric nanogenerator for harvesting wind energy and as self-powered wind vector sensor system, ACS Nano 13 (2013) 847–853, https://doi.org/10.1021/nn4043157.
[29] Y. Xie, S. Wang, L. Lin, Q. Jing, Z.H. Lin, S. Niu, Z. Wu, Z.L. Wang, Rotary triboelectric nanogenerator based on a hybridized mechanism for harvesting wind energy, ACS Nano 7 (2013) 7119–7125, https://doi.org/10.1021/nn402477h.
[30] M.L. Seol, J.H. Woo, S.B. Jeon, D. Kim, S.J. Park, J. Hur, Y.K. Choi, Vertically stacked thin triboelectric nanogenerator for wind energy harvesting, Nano Energy 14 (2015) 201–208, https://doi.org/10.1016/j.nanoen.2014.11.016.
[31] Z. Zhao, X. Pu, C. Du, L. Li, C. Jiang, W. Hu, Z.L. Wang, Freestanding flag-type triboelectric nanogenerator for harvesting high-altitude wind energy from arbitrary directions, ACS Nano (2016), https://doi.org/10.1021/acsnano.5b07157.
[32] Q. Liang, X. Yan, X. Liao, Y. Zhang, Integrated multi-unit transparent triboelectric nanogenerator harvesting rain power for driving electronics, Nano Energy 6 (2016) 29084, https://doi.org/10.1016/j.nanoen.2016.04.033.
[33] Y.C. Lai, Y.C. Hsiao, H.M. Wu, Z.L. Wang, Waterproof Fabric-Based Multifunctional Triboelectric Nanogenerator for Universally Harvesting Energy from Raindrops, Wind, and Human Motions and as Self-Powered Sensors, Adv. Sci. (2019), https://doi.org/10.1002/advs.201801883.
[34] H.R. Zhu, W. Tang, C.Z. Gao, Y. Han, T. Li, X. Cao, Z.L. Wang, Self-powered metal surface anti-corrosion protection using energy harvested from rain drops and wind, Nano Energy (2014), https://doi.org/10.1016/j.nanoen.2014.11.041.
[35] X. Wang, S. Niu, Y. Yin, F. Yi, Z. You, Z.L. Wang, Triboelectric nanogenerator based on fully enclosed rolling spherical structure for harvesting low-frequency water wave energy, Adv. Energy Mater. 9 (2015) 4553–4562, https://doi.org/10.1002/aenm.201501467.
[36] L. Xu, T. Jiang, P. Lin, J.J. Shao, C. He, W. Zhong, X.Y. Chen, Z.L. Wang, Coupled triboelectric nanogenerator networks for efficient water wave energy harvesting, ACS Nano (2018), https://doi.org/10.1021/acsnano.7b08674.
[37] G. Zhu, Y.S. Zhou, P. Bai, X.S. Meng, Q. Jing, J. Chen, Z.L. Wang, A shape-adaptive thin-film-based approach for 50% high-efficiency energy generation through micro-grating sliding electrification, Adv. Mater. 102 (2014) 2491–2501, https://doi.org/10.1002/adma.201400021.
[38] Y. Xie, S. Wang, S. Niu, L. Lin, Q. Jing, J. Yang, Z. Wu, Z.L. Wang, Grating-structured freestanding triboelectric-layer nanogenerator for harvesting mechanical energy at 85% total conversion efficiency, Adv. Mater. 26 (2014) 6599–6607, https://doi.org/10.1002/adma.201402428.
[39] C. Ning, L. Tian, X. Zhao, S. Xiang, Y. Tang, E. Liang, Y. Mao, Washable textile-structured single-electrode triboelectric nanogenerator for self-powered wearable electronics, J. Mater. Chem. A. 6 (2018) 19143–19150, https://doi.org/10.1039/c8ta07784c.
[40] J.N. Kim, J. Lee, T.W. Go, A. Rajabi-Abhari, M. Mahato, J.Y. Park, H. Lee, I.K. Oh, Skin-attachable and biofriendly chitosan-diatom triboelectric nanogenerator, Nano Energy 75 (2020), 104904, https://doi.org/10.1016/j.nanoen.2020.104904.
[41] J. Chun, B.U. Ye, J.W. Lee, D. Choi, C.Y. Kang, S.W. Kim, Z.L. Wang, J.M. Baik, Boosted output performance of triboelectric nanogenerator via electric double layer effect, Nat. Commun. 7 (2016) 12985, https://doi.org/10.1038/ncomms12985.
[42] Z. Lin, J. Chen, X. Li, Z. Zhou, K. Meng, W. Wei, J. Yang, Z.L. Wang, Triboelectric nanogenerator enabled body sensor network for self-powered human heart-rate monitoring, ACS Nano 11 (2017) 8830–8837, https://doi.org/10.1021/acsnano.7b02975.
[43] S. Niu, X. Wang, F. Yi, Y.S. Zhou, Z.L. Wang, A universal self-charging system driven by random biomechanical energy for sustainable operation of mobile electronics, Nat. Commun. 6 (2015) 8975, https://doi.org/10.1038/ncomms9975.
[44] X. Cheng, L. Miao, Y. Song, Z. Su, H. Chen, X. Chen, J. Zhang, H. Zhang, High efficiency power management and charge boosting strategy for a triboelectric nanogenerator, Nano Energy 38 (2017) 438–446, https://doi.org/10.1016/j.nanoen.2017.05.063.
[45] K. Dong, Z. Wu, J. Deng, A.C. Wang, H. Zou, C. Chen, D. Hu, B. Gu, B. Sun, Z. L. Wang, A stretchable yarn embedded triboelectric nanogenerator as electronic skin for biomechanical energy harvesting and multifunctional pressure sensing, Adv. Mater. 30 (2018) 1–12, https://doi.org/10.1002/adma.201804944.
[46] S. Li, J. Wang, W. Peng, L. Lin, Y. Zi, S. Wang, G. Zhang, Z.L. Wang, Sustainable energy source for wearable electronics based on multilayer elastomeric triboelectric nanogenerators, Adv. Energy Mater. (2017), https://doi.org/10.1002/aenm.201602832.
[47] W. Seung, M.K. Gupta, K.Y. Lee, K.S. Shin, J.H. Lee, T.Y. Kim, S. Kim, J. Lin, J. H. Kim, S.W. Kim, Nanopatterned textile-based wearable triboelectric nanogenerator, ACS Nano 9 (2015) 3501–3509, https://doi.org/10.1021/nn507221f.
[48] J. Chen, W. Xuan, P. Zhao, U. Farooq, P. Ding, W. Yin, H. Jin, X. Wang, Y. Fu, S. Dong, J. Luo, Triboelectric effect based instantaneous self-powered wireless sensing with self-determined identity, Nano Energy 51 (2018) 1–9, https://doi.org/10.1016/j.nanoen.2018.06.029.
[49] C. Fang, T. Tong, T. Bu, Y. Cao, S. Xu, Y. Qi, C. Zhang, Overview of power management for triboelectric nanogenerators, Adv. Intell. Syst. 2 (2020), 1900129, https://doi.org/10.1002/aisy.201900129.
[50] P. Vasandani, B. Gattu, Z.H. Mao, W. Jia, M. Sun, Using a synchronous switch to enhance output performance of triboelectric nanogenerators, Nano Energy 43 (2018) 210–218, https://doi.org/10.1016/j.nanoen.2017.11.027.
[51] H. Qin, G. Cheng, Y. Zi, G. Gu, B. Zhang, W. Shang, F. Yang, J. Yang, Z. Du, Z. L. Wang, High energy storage efficiency triboelectric nanogenerators with unidirectional switches and passive power management circuits, Adv. Funct. Mater. 28 (2018), https://doi.org/10.1002/adfm.201805216.
[52] J. Yang, F. Yang, L. Zhao, W. Shang, H. Qin, S. Wang, X. Jiang, G. Cheng, Z. Du, Managing and optimizing the output performances of a triboelectric nanogenerator by a self-powered electrostatic vibrator switch, Nano Energy 46 (2018) 220–228, https://doi.org/10.1016/j.nanoen.2018.02.013.
[53] H. Qin, G. Gu, W. Shang, H. Luo, W. Zhang, P. Cui, B. Zhang, J. Guo, G. Cheng, Z. Du, A universal and passive power management circuit with high efficiency for pulsed triboelectric nanogenerator, Nano Energy 68 (2020), 104372, https://doi.org/10.1016/j.nanoen.2019.104372.
[54] Z. Liu, M. Muhammad, L. Cheng, E. Xie, W. Han, Improved output performance of triboelectric nanogenerators based on polydimethylsiloxane composites by the capacitive effect of embedded carbon nanotubes, Appl. Phys. Lett. 117 (2020), 143903, https://doi.org/10.1063/5.0025001.
[55] Q. Guo, X. Yang, Y. Wang, W. Xu, J. Duan, Q. Tang, Dielectric Hole Collector toward Boosting Charge Transfer of CsPbBr3 Hybrid Nanogenerator by Coupling Triboelectric and Photovoltaic Effects, Adv. Funct. Mater. 2101348 (2021) 1–11, https://doi.org/10.1002/adfm.202101348.
[56] Z. Zhang, Y. Chen, D.K. Debeli, J.S. Guo, Facile method and novel dielectric material using a nanoparticle-doped thermoplastic elastomer composite fabric for triboelectric nanogenerator applications, ACS Appl. Mater. Interfaces (2018), https://doi.org/10.1021/acsami.8b02133.
[57] X. Xia, J. Chen, H. Guo, G. Liu, D. Wei, Y. Xi, X. Wang, C. Hu, Embedding variable micro-capacitors in polydimethylsiloxane for enhancing output power of triboelectric nanogenerator, Nano Res 10 (2017) 320–330, https://doi.org/10.1007/s12274-016-1294-4.
[58] B.D. Chen, W. Tang, C. Zhang, L. Xu, L.P. Zhu, L.J. Yang, C. He, J. Chen, L. Liu, T. Zhou, Z.L. Wang, Au nanocomposite enhanced electret film for triboelectric nanogenerator, Nano Res 11 (2018) 4890–4904, https://doi.org/10.1007/s12274-017-1716-y.
[59] X. He, H. Guo, X. Yue, J. Gao, Y. Xi, C. Hu, Improving energy conversion efficiency for triboelectric nanogenerator with capacitor structure by maximizing surface charge density, Nanoscale 7 (2015) 1896–1903, https://doi.org/10.1039/c4nr05512h.
[60] M.S. Rasel, P. Maharjan, M. Salauddin, M.T. Rahman, H.O. Cho, J.W. Kim, J. Y. Park, An impedance tunable and highly efficient triboelectric nanogenerator for large-scale, ultra-sensitive pressure sensing applications, Nano Energy 49 (2018) 603–613, https://doi.org/10.1016/j.nanoen.2018.04.060.
[61] H. Wang, M. Shi, K. Zhu, Z. Su, X. Cheng, Y. Song, X. Chen, Z. Liao, M. Zhang, H. Zhang, High performance triboelectric nanogenerators with aligned carbon nanotubes, Nanoscale 8 (2016) 18489–18494, https://doi.org/10.1039/c6nr06319e.
[62] D. Wang, Y. Lin, D. Hu, P. Jiang, X. Huang, Multifunctional 3D-MXene/PDMS nanocomposites for electrical, thermal and triboelectric applications, Compos. Part A Appl. Sci. Manuf. 130 (2020), 105754, https://doi.org/10.1016/j.compositesa.2019.105754.
[63] K. Parida, J. Xiong, X. Zhou, P.S. Lee, Progress on triboelectric nanogenerator with stretchability, self-healability and bio-compatibility, Nano Energy 59 (2019) 237–257, https://doi.org/10.1016/j.nanoen.2019.01.077.
[64] C. Pan, D. Liu, M.J. Ford, C. Majidi, Ultrastretchable, wearable triboelectric nanogenerator based on sedimented liquid metal elastomer composite, Adv. Mater. Technol. 5 (2020) 1–8, https://doi.org/10.1002/admt.202000754.
[65] H. Chen, Y. Xu, L. Bai, Y. Jiang, J. Zhang, C. Zhao, T. Li, H. Yu, G. Song, N. Zhang, Q. Gan, Crumpled graphene triboelectric nanogenerators: smaller devices with higher output performance, Adv. Mater. Technol. (2017), https://doi.org/10.1002/admt.201700044.
[66] M. Weber, M.R. Kamal, Estimation of the volume resistivity of conductive fiber composites by two new models, Annu. Tech. Conf. - ANTEC, Conf. Proc. 2 (1997) 2357–2361, https://doi.org/10.1016/b978-188420777-8.50010-2.
[67] M. Moniruzzaman, K.I. Winey, Polymer nanocomposites containing carbon nanotubes, Macromolecules 39 (2006) 5194–5205, https://doi.org/10.1021/ma060733p.

[68] X. Zhao, J. Dhanani, Z. Ounaies, O. Rashwan, On the effects of electrical conductivity on the triboelectric behavior of a PDMS-based composite material, : ASME 2020 Conf. Smart Mater. Adapt. Struct. Intell. Syst. SMASIS 2020 (2020), https://doi.org/10.1115/SMASIS20-2300.
[69] P. Vasandani, Z.H. Mao, W. Jia, M. Sun, Relationship between triboelectric charge and contact force for two triboelectric layers, J. Electro 90 (2017) 147–152, https://doi.org/10.1016/j.elstat.2017.11.001.
[70] G. Zhu, B. Peng, J. Chen, Q. Jing, Z. Lin Wang, Triboelectric nanogenerators as a new energy technology: From fundamentals, devices, to applications, Nano Energy (2014), https://doi.org/10.1016/j.nanoen.2014.11.050.
[71] R. Chen, X. Xu, D. Yu, C. Xiao, M. Liu, J. Huang, T. Mao, C. Zheng, Z. Wang, X. Wu, Highly stretchable and fatigue resistant hydrogels with low Young's modulus as transparent and flexible strain sensors, J. Mater. Chem. C. (2018), https://doi.org/10.1039/c8tc02583e.
[72] Y. Liu, M. Pharr, G.A. Salvatore, Lab-on-Skin: A Review of Flexible and Stretchable Electronics for Wearable Health Monitoring, ACS Nano 38 (2017) 1236–1247, https://doi.org/10.1021/acsnano.7b04898.
[73] K. Subramaniam, A. Das, G. Heinrich, Development of conducting polychloroprene rubber using imidazolium based ionic liquid modified multi-walled carbon nanotubes, Compos. Sci. Technol. 71 (2011) 1441–1449, https://doi.org/10.1016/j.compscitech.2011.05.018.
[74] Q. Yin, Y. Wen, H. Jia, L. Hong, Q. Ji, Z. Xu, Enhanced mechanical, dielectric, electrical and thermal conductive properties of HXNBR/HNBR blends filled with ionic liquid-modified multiwalled carbon nanotubes, J. Mater. Sci. 52 (2017) 10814–10828, https://doi.org/10.1007/s10853-017-1251-y.
[75] L. Zhao, Y. Li, X. Cao, J. You, W. Dong, Multifunctional role of an ionic liquid in melt-blended poly(methylmethacrylate)/ multi-walled carbon nanotube nanocomposites, Nanotechnology 23 (2012), 255702, https://doi.org/10.1088/0957-4484/23/25/255702.
[76] K. Oh, J.Y. Lee, S.S. Lee, M. Park, D. Kim, H. Kim, Highly stretchable dielectric nanocomposites based on single-walled carbon nanotube/ionic liquid gels, Compos. Sci. Technol. 83 (2013) 40–46, https://doi.org/10.1016/j.compscitech.2013.04.004.
[77] K. Subramaniam, A. Das, F. Simon, G. Heinrich, Networking of ionic liquid modified CNTs in SSBR, Eur. Polym. J. 49 (2013) 345–352, https://doi.org/10.1016/j.eurpolymj.2012.10.023.
[78] K. Subramaniam, A. Das, D. Steinhauser, M. Klüppel, G. Heinrich, Effect of ionic liquid on dielectric, mechanical and dynamic mechanical properties of multi-walled carbon nanotubes/polychloroprene rubber composites, Eur. Polym. J. 47 (2011) 2234–2243, https://doi.org/10.1016/j.eurpolymj.2011.09.021.
[79] T.A. Kim, H.S. Kim, S.S. Lee, M. Park, Single-walled carbon nanotube/silicone rubber composites for compliant electrodes, Carbon N. Y 50 (2012) 444–449, https://doi.org/10.1016/j.carbon.2011.08.070.
[80] A.F. Diaz, R.M. Felix-Navarro, A semi-quantitative tribo-electric series for polymeric materials: The influence of chemical structure and properties, J. Electro 62 (2004) 277–290, https://doi.org/10.1016/j.elstat.2004.05.005.
[81] J. Kiefer, J. Fries, A. Leipertz, Experimental vibrational study of imidazolium-based ionic Liquids: Raman and infrared spectra of 1-ethyl-3methylimidazolium bis (trifluoromethylsulfonyl) imide and 1-ethyl-3-methylimidazolium ethylsulfate, Appl. Spectrosc. 61 (2007) 1306–1311, https://doi.org/10.1366/000370207783292000.
[82] H. Kang, H. Kim, S. Kim, H.J. Shin, S. Cheon, J.H. Huh, D.Y. Lee, S. Lee, S.W. Kim, J.H. Cho, Mechanically Robust Silver Nanowires Network for Triboelectric Nanogenerators, Adv. Funct. Mater. 26 (2016) 7717–7724, https://doi.org/10.1002/adfm.201603199.

Xiaoyue Zhao is currently a PhD student in Mechanical Engineering at Penn State-University Park. She received a BEng in Process Equipment & Control Engineering from Xi'an Jiaotong University in 2015 and a MSc in Mechanical Engineering from Carnegie Mellon University in 2017. She worked as a reliability engineer at Amazon before joining the EMCLab at Penn State. Her research interests include the triboelectric behavior of smart materials and energy harvesting.

Zoubeida Ounaies is a professor of mechanical engineering and director of the Convergence Center for Living Multifunctional Material Systems (LiMC^2) at the Pennsylvania State University. She joined Penn State in January 2011, where she established the Electroactive Materials Characterization Laboratory (EMCLab), where her students and she focus on advancing the application of smart materials in energy storage, energy conversion and energy harvesting. She is associate editor of the Journal of *Intelligent Materials Systems and Structures* and the *Smart Materials and Structures* Journal, and a fellow of ASME and SPIE.